IEEE Photonics Journal
An IEEE Photonics Society Publication

Open Access

Highly Nonlinear Organic-Silicon Slot Waveguide for Ultrafast Multimode All-Optical Logic Operations

Volume 12, Number 6, December 2020

Yonghua Wang
Haofan Yang
Wenchan Dong
Lei Lei
Jing Xu
Xinliang Zhang, *Senior Member, IEEE*
Ping Xu

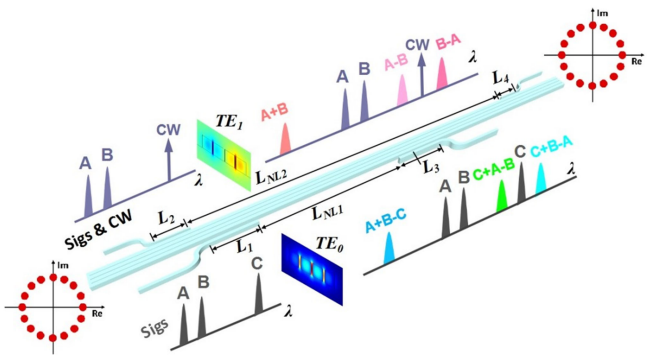

DOI: 10.1109/JPHOT.2020.3040967

Highly Nonlinear Organic-Silicon Slot Waveguide for Ultrafast Multimode All-Optical Logic Operations

Yonghua Wang [1], Haofan Yang [2], Wenchan Dong [2,3], Lei Lei [1], Jing Xu [2,3], Xinliang Zhang [2,3], *Senior Member, IEEE*, and Ping Xu [1]

[1]College of Physics and Optoelectronic Engineering, Shenzhen University, Shenzhen 518060, China
[2]School of Optical and Electronic Information, Huazhong University of Science and Technology, Wuhan 430074, China
[3]Wuhan National Laboratory for Optoelectronics, Huazhong University of Science and Technology, Wuhan 430074, China

DOI:10.1109/JPHOT.2020.3040967

Manuscript received August 17, 2020; revised November 14, 2020; accepted November 24, 2020. Date of publication December 2, 2020; date of current version December 9, 2020. This work was supported in part by the National Key Research and Development Program of China under Grants 2019YFB2203102 and 2017YFA0305200, in part by the National Natural Science Foundation of China (NSFC) under Grants 61275167, 61805151, and 61775063, in part by the Natural Science Foundation of Guangdong Province under Grants 2020A1515011492 and 2017A030310131, in part by Basic Research Program of Shenzhen under Grants JCYJ20170302151033006, JCYJ2017081701827765, and JCYJ20170817111349280, and in part by China Postdoctoral Science Foundation under Grant 2020M672783. *(Yonghua Wang and Haofan Yang contributed equally to this work.)* Corresponding authors: Lei Lei; Jing Xu (e-mail: leilei@szu.edu.cn; jing_xu@hust.edu.cn).

Abstract: Highly nonlinear multimode optical integrated devices hold great promise for the emerging large-capacity mode division multiplexing (MDM) technology, and they correspondingly enable multimode optical signal processing at nodes of the MDM network. Here, we propose a highly nonlinear multimode organic-silicon slot waveguide (HN-OSSW) whose nonlinearity is greatly improved by the intensive optical field confinement in the nano-gaps filled with highly nonlinear organic material. Specifically, the achieved nonlinear coefficients of the HN-OSSW under TE_0 and TE_1 modes are estimated higher than 7000 $W^{-1}m^{-1}$ and 5800 $W^{-1}m^{-1}$, respectively. Also, by phase mismatch optimization, this nanostructure exhibits superior intramode four-wave mixing conversion efficiency but ignorable intermode crosstalk. Coupling efficiency of the mode multiplexer and the optimal nonlinear interaction length are discussed in detail. Based on the HN-OSSW, we then numerically demonstrate a multimode all-optical hexadecimal addition and subtraction for sixteen phase-shift keying (16PSK) signals with the operation rate of 1.28Tb/s. Six different logic operations including A+B-C, A+C-B, B+C-A, A+B, A-B and B-A are simultaneously obtained with good performance evaluations, indicating the promising prospect of the HN-OSSW applied in ultrafast multimode signal processing.

Index Terms: Integrated optical devices, multimode waveguide, slot waveguide, organic material, four wave mixing, optical logic operation.

1. Introduction

The newly emerging large-capacity optical transmission strategy mode-division multiplexing (MDM) is expected as a viable way to improve the capacity crunch but with a more reasonable cost compared to the optical time division multiplexing (OTDM) and dense wavelength division multiplexing (DWDM) [1]. Correspondingly, multimode optical signal processing based on nonlinear devices is required at nodes of the MDM system. Traditional technology such as multimode fiber [2]–[5] offers an effective way for multimode optical signal processing but suffers from the inability to large-scale integration. Instead, multimode silicon photonic devices [6]–[8] have attracted increasing attentions not only owing to their intrinsic capability for multimode signal processing, but also the advantages of compact footprint, compatibility with metal-oxide-semiconductor (CMOS) platform, robustness and low cost for the mass production [9]–[12].

On the other hand, among the all-optical signal processing technologies, all-optical logic operation is expected to play an important role in optical communications. Specifically, on different layers of the optical network, optical logic function can be widely applied for optical format conversion [13], wavelength conversion [14], [15], demultiplexing [16], sampling [17], decision [18], reshaping [19], etc. Besides, optical logic operation is also one of the crucial methods for optical high-performance computing, exhibiting the outstanding features of parallel processing, ultra-high processing speed and low power consumption. More recently, it has also shown great potential for utilization in optical programmable devices [20], [21] and artificial intelligence [22]. Thus, it would be very attractive and meaningful to find an integrated strategy for all-optical multimode logic operation that may further improve the computing efficiency in MDM system.

Recent works based on silicon strip waveguides have demonstrated a 10Gb/s multimode all-optical AND logic gate for return-to-zero (RZ) signals [23] and 40 Gb/s mode-selective wavelength conversion for carrier-suppressed return-to-zero (CSRZ) signal. In particular, the conversion process in the latter is indeed realized by an AND logic operation between the input CSRZ signal and a continuous wave (CW) [24]. The operation speed is then increased to 102.6Gb/s for OFDM-QPSK signals [25] by the same group. These works are the pioneering researches on multimode optical signal processing. However, more effort can be anticipated to further improve the nonlinear response restriction, caused by the material and structure, for a higher speed multimode operation.

In this work, we propose a highly nonlinear organic-silicon slot waveguide (HN-OSSW) for 1.28Tb/s all-optical multimode hexadecimal addition and subtraction. With the highly nonlinear organic cladding and optical field enhancement in the narrow gaps, the nonlinear coefficients of the HN-OSSW under TE_0 and TE_1 modes are respectively estimated exceeding 7000 $W^{-1}m^{-1}$ and 5800 $W^{-1}m^{-1}$. In addition, in order to obtain the optimum logic conversion efficiency, which is affected by the overall accumulated nonlinear response, coupling efficiency of the mode multiplexer, phase match condition and nonlinear interaction distance of the HN-OSSW are all discussed in detail. Based on the proposed HN-OSSW, we numerically demonstrate an all-optical multimode hexadecimal addition and subtraction for sixteen phase-shift keying (16PSK) signals with the operation rate of 1.28Tb/s. Six different 16-ary logic operations are simultaneously achieved in TE_0 (A+B-C, A+C-B and B+C-A) and TE_1 modes (A+B, A-B and B-A). Error vector magnitudes (EVMs) and optical signal-to-noise ratios (OSNRs) are calculated and analyzed for performance evaluation.

Apart from the intrinsic advantage of being compatible with the MDM system at nodes, our proposal features several other improvements compared to those reported schemes. (1) The nonlinear coefficients of both modes greatly increase associated with the high nonlinear organic cladding and tight field confinement within nano-gaps. (2) The increased nonlinearity allows a faster operation speed, lower input power as well as more compact device size, which is favorable for large-scale integration. (3) The proposed nanostructure can totally replace the logic element in the canonical logic units-based programmable logic array (CLUs-PLA) proposed in our previous work [26], [27]. Considering the multimode processing, the computing capacity would be further improved to create a high-performance optical computing.

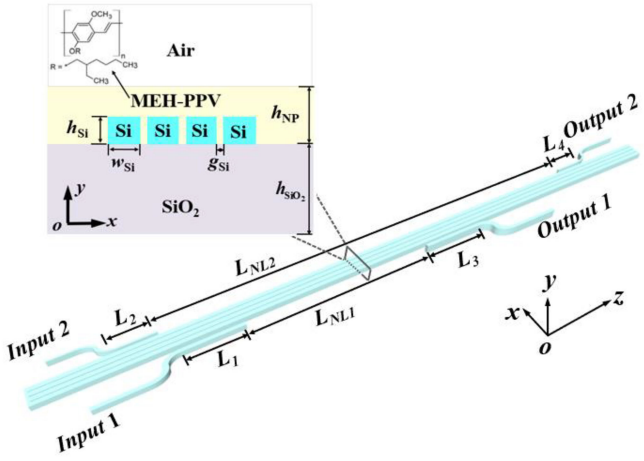

Fig. 1. Schematic diagram of the highly nonlinear organic-silicon slot waveguide (HN-OSSW). $h_{\rm si} = 220$ nm, $w_{\rm si} = 220$ nm, $g_{\rm si} = 50$ nm, $h_{\rm NP} = 500$ nm.

2. Device Design

2.1 Device Configuration of the HN-OSSW

Illustrated in Fig. 1 is the proposed HN-OSSW that we use for multimode optical hexadecimal logic operations. The HN-OSSW is composed of four parallel silicon rib waveguides with each narrow gap ($g_{\rm si}$) of 50 nm. The slot waveguide is 220 nm in height ($h_{\rm si}$), which is identical to the width of each rib waveguide ($w_{\rm si}$). Here, a 500 nm thick 2-methoxy-5-(2-ethylhexyloxy)-1,4-phenylenevinylene (MEH-PPV) [28] is applied as a cladding. With this nanostructure, two propagation modes, i.e., TE_0 and TE_1, can be efficiently excited by the input signals through the directional couplers (DCs), which perform as mode multiplexers at the input, while mode demultiplexers at the output. As shown in the Fig. 1, L_1 and L_2 respectively denote the effective coupling lengths ($L_{\rm eff}$) of multiplexing for TE_0 and TE_1 modes, while L_3 and L_4 accordingly denote those of the demultiplexing. The SOI multimode slot waveguide can be fabricated by standard electron beam lithography (EBL) and inductively coupled plasma etching (ICP), which are totally compatible with the CMOS manufacturing platform. Also, with the help of spin-coating and vacuuming, the organic MEH-PPV would be well cladded on the waveguide and filled in the gaps. Note that the gap width designed as 50 nm here is possible to be further narrowed to about 10 nm with the "sequential fabrication approach" as reported in [29]. Thanks to the phase mismatch optimization, intramode FWM highly occurs in the nonlinear functional zone with the length of $L_{\rm NL}$ ($L_{\rm NL1}$ for TE_0 and $L_{\rm NL2}$ for TE_1) to complete the logic operations, while the intermode crosstalk is ignorable. Filtering and signal analysis are followed at each output of the device to further evaluate the logic operation performance obtained from the FWM idlers.

2.2 Mode Analysis and Nonlinear Coefficients

Slot waveguide has been widely reported as a feasible strategy for nonlinearity enhancement and nonlinear optical signal processing since the energy can be intensively confined in a very narrow gap [29]. So far, most of the reported works have mainly focused on single-slot nanostructure [28]–[31], where TE_0 or TM_0 mode is usually excited to carry the information. Compared to those reported works, our proposal is able to simultaneously achieve two propagation modes (i.e., TE_0 and TE_1) as the electric field distributions $E_{\rm x}$ shown in Fig. 2(a) and 2(b), exhibiting the compatibility with the multimode signal processing requirement of the MDM system. Fig. 2(c) and 2(d) show the corresponding normalized magnitude of $E_{\rm x}$. One can clearly see that the light is tightly confined in the nanoscale nonlinear organic slots. This well-confined light together with the large nonlinear

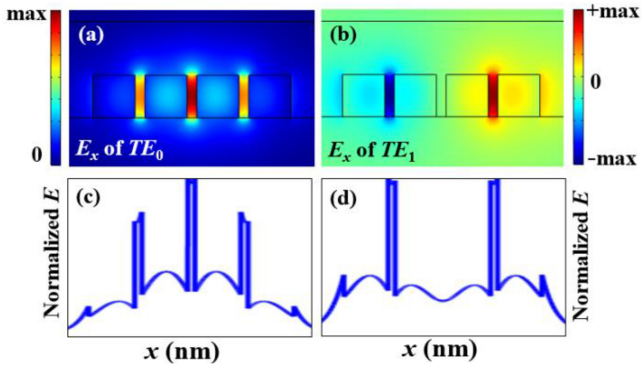

Fig. 2. Electric field distributions in the HN-OSSW. (a) E_x of TE_0 mode. (b) E_x of TE_1 mode. (c) Normalized magnitude of electric field for TE_0 mode. (d) Normalized magnitude of electric field for TE_1 mode.

TABLE 1
Parameters for the Calculation of Effective Nonlinear Coefficients

Material	n	n_2 (m^2/W)	A_{eff_TE0} (μm^2)	A_{eff_TE1} (μm^2)
MEH-PPV	1.65	2×10^{-16}	0.03587	0.04365
Si	3.48	5.3×10^{-18}	0.0899	0.01143
SiO_2	1.48	4.7×10^{-20}	0.01447	0.01781

index of slot material provides further enhanced nonlinearity which potentially could be used for ultrafast high-performance optical computing and signal processing.

The nonlinear characteristic of the HN-OSSW is estimated for each material section in the waveguide and scaled by the respective fractional energy of the mode in the material $E_{f,q}$. The effective nonlinear coefficient γ_{eff} of the HN-OSSW then reads [32]

$$\gamma_{\text{eff}} = \sum \gamma_q \times E_{f,q} \tag{1}$$

with γ_q defined as:

$$\gamma_q = \frac{\omega n_2}{c A_{\text{eff}}} \tag{2}$$

where ω is the angular frequency of the incident light, n_2 is the Kerr index of the material and A_{eff} denotes the effective mode area in the material as defined A_1 by [33]. In the C-band around 1550 nm, we use the following parameters [32], [34] to calculate γ_{eff} of both TE_0 and TE_1 modes, including the effective mode areas, Kerr indices and refraction indices of MEH-PPV, silicon and silica.

It is seen from Table 1 that the Kerr index of the nonlinear polymer MEH-PPV is 2×10^{-16} m^2/W [34], which shows a 40-fold increase compared to that of the silicon. This material's excellent optical nonlinear property together with the energy enhancement in the nanoscale slots promises that the nonlinear coefficients of our HN-OSSW are much higher than those of the common strip silicon waveguide. Specifically, our nanostructure provides the nonlinear coefficients of TE_0 and TE_1 modes reaching to 7078 $W^{-1}m^{-1}$ (γ_{eff_TE0}) and 5858 $W^{-1}m^{-1}$ (γ_{eff_TE1}), respectively.

Fig. 3(a) and 3(b) illustrate the nonlinear coefficient evolutions of both modes as the gap and rib widths change. Generally, as TE_0 mode confines more energy in the slots, it exhibits a higher nonlinearity response under both situations. Consistent with this, it is apparent that the slot width dominantly affects the nonlinear coefficients of the HN-OSSW due to the strong optical intensity. Also in both cases, the nonlinear coefficients obviously rise as the gap and rib get narrower since

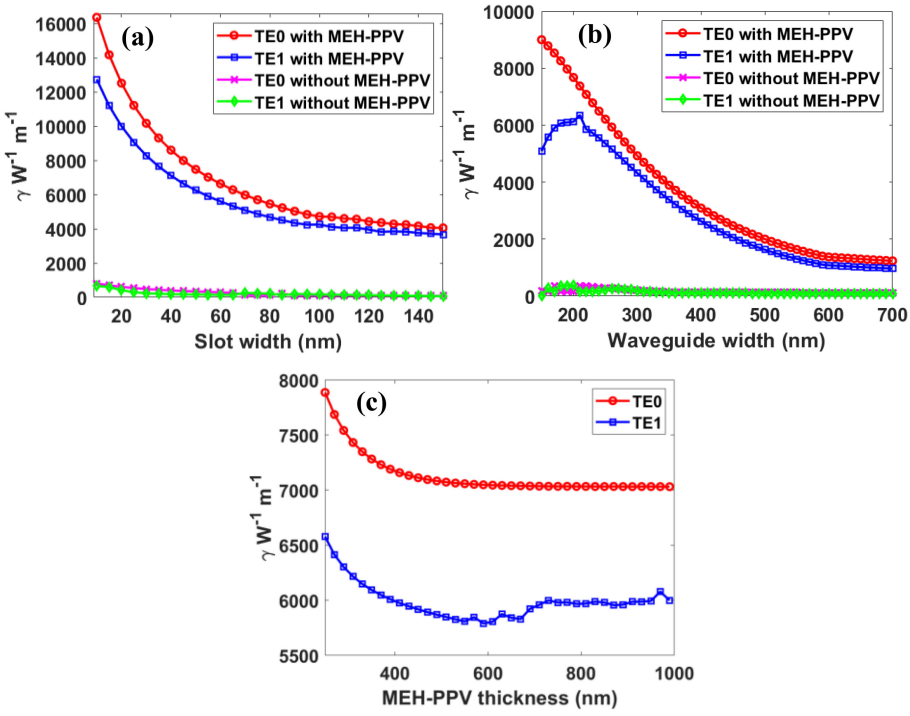

Fig. 3. Nonlinear coefficients of TE_0 and TE_1 modes with different (a) slot widths, (b) rib waveguide widths, and (c) MEH-PPV thicknesses.

the effective mode areas shrink. However, as shown in Fig. 3(b), this trend turns to be invalid as the rib width is less than 200 nm, where can be found an irregular variation because the TE_1 mode cannot be well excited when the silicon rib is too narrow. Considering the practical fabrication technology, the width of the silicon rib is set as 220 nm to obtain two propagation modes while simultaneously maintain the high nonlinear coefficients. Compared to the proposed HN-OSSW, nonlinear coefficients of the nanostructure without the organic cladding are very low for both modes as displayed in the magenta and cyan lines, indicating that the organic material plays a more important role in improving the nonlinear character of the HN-OSSW rather than the slot configuration. Result in Fig. 3(c) shows that the effect of polymer thickness on the nonlinear coefficients is lesser. When the polymer is thicker than 500 nm, the nonlinear coefficients under both modes are with slight variation cause A_{eff} in the polymer is no longer increasing.

2.3 Phase Mismatch

Apart from the high nonlinear coefficients, phase matching condition is also indispensable to the high-performance multimode FWM, which enables an efficient FWM between the interacting waves within the same modes whereas a slight interaction between different modes. In our proposal, since the slot width is the major factor to influence the nonlinear coefficients, we investigate the phase mismatch features by tailoring the HN-OSSW with various slot widths. The width of rib waveguide and height of each layer remain unchanged as aforementioned. Here, based on ITU grid, signal A places at 1535.6 nm (λ_{A}) and signal C (λ_{C}) places at 1571.6 nm. Based on non-degenerate FWM, the phase mismatch defined as $\Delta\beta = \beta_{\mathrm{sigA}}+\beta_{\mathrm{sigC}}-\beta_{\mathrm{sigB}}$-$\beta_{\mathrm{idler}}$ is investigated as a function of the wavelength of signal B (λ_{B}), where β_{sigA}, β_{sigB}, β_{sigC} and β_{idler} are the respective propagation constants of the three input pump signals and the idler with the wavelength of $\lambda_{\mathrm{A}}+\lambda_{\mathrm{C}}$-$\lambda_B$. One needs to tailor the dispersion of the HN-OSSW so that the intramode phase mismatch is as small

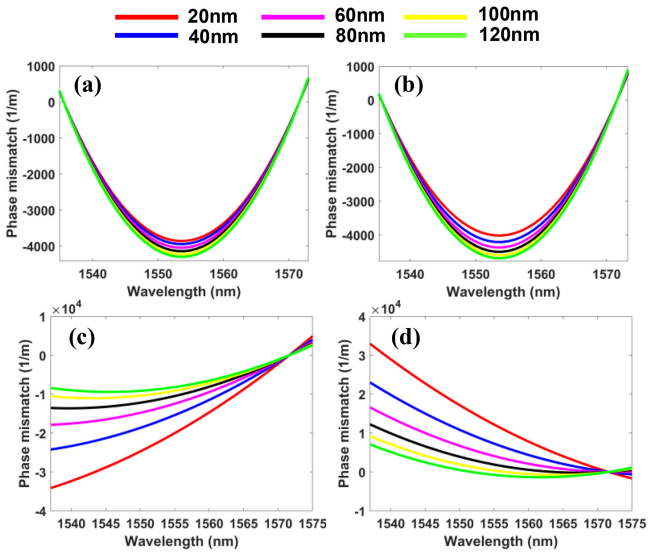

Fig. 4. Phase mismatch with different slot widths for (a) TE_0 mode, (b) TE_1 mode, (c) signal A and idler on TE_1 mode, signal B and C on TE_0 mode, and (d) signal A and idler on TE_0 mode, signal B and C on TE_1 mode.

as possible, meanwhile, maintain a comparatively small dimension for the intensive optical energy confinement. On the contrary, the intermode phase mismatch should be large in a wide band in order to prevent the crosstalk. In Fig. 4(a) and 4(b), it is seen that the phase mismatch curves within TE_0 and TE_1 modes are relatively low and nearly overlap in the C band, which is beneficial to improve the fabrication error tolerance. Conversely, the intermode phase mismatch displayed in Fig. 4(c) and 4(d) dramatically rises as the gap width gets narrower. Here, signal A and C are on one mode, while signal B and the idler are on the other. One can find that with the 50 nm gap width, it is reasonable to ignore the crosstalk between TE_0 and TE_1 modes due to the large phase mismatch. This would be further demonstrated by the optical spectra of the intermode FWM shown in section 3.

2.4 Directional Couplers for Mode Multiplexing and Demultiplexing

Mode multiplexing and demultiplexing can be achieved thanks to the directional couplers, which are investigated and optimized based on finite difference time domain (FDTD) approach. According to the coupling mode theory [35], when light is launched into the access waveguide port, it excites equally the even and odd supermodes, which then propagate with different velocities. As the phase difference between these two supermodes reaches to π, the light is completely transferred to the adjacent waveguide. In our work, the widths of DC access waveguides are 348 nm for TE_0 mode and 294 nm for TE_1 mode, respectively. In both cases, the gap between the access waveguide and slot waveguide is set as 200 nm. As shown in Fig. 5(a) and 5(b), with different proper coupling lengths, both TE_0 and TE_1 modes are well excited in the HN-OSSW, displaying the feasibility of DC for mode multiplexing and demultiplexing. Coupling efficiencies are then assessed and illustrated in Fig. 5(c). For each mode, the coupling efficiency in most of the C band is higher than 0.9 and nearly perfect around 1550 nm. Even though progressive deterioration can be found in the S and L bands, the coupling efficiencies are still exceeding 0.72 and 0.97 for TE_0 and TE_1 modes, respectively.

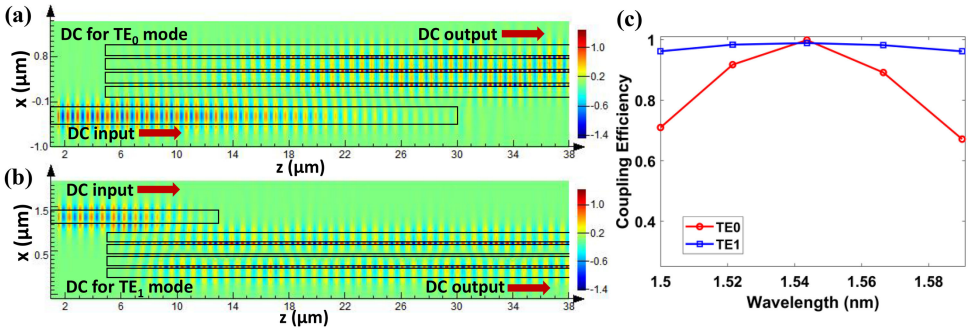

Fig. 5. (a)-(b) Mode multiplexing in the HN-OSSW through directional couplers. (c) Coupling efficiencies under TE_0 and TE_1 modes.

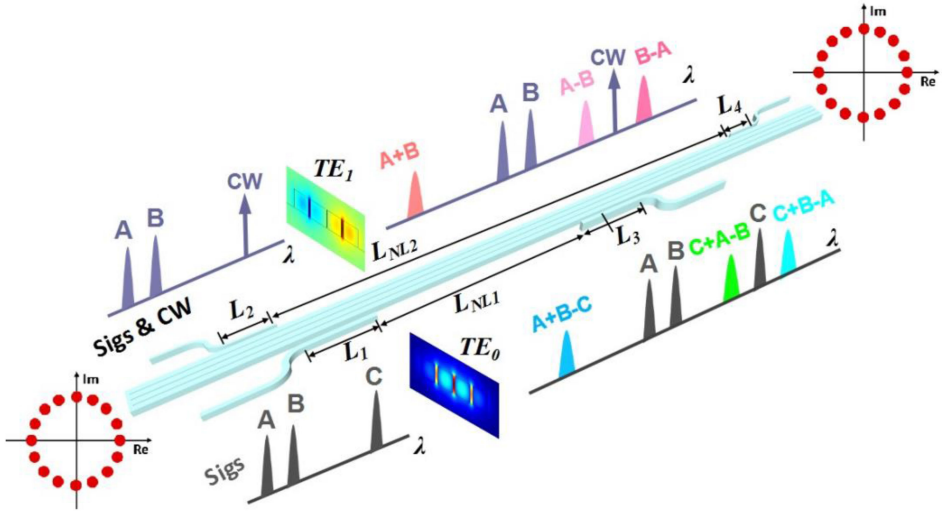

Fig. 6. Principle of the 1.28Tb/s all-optical multimode hexadecimal addition and subtraction in HN-OSSW.

3. 1.28Tb/s All-Optical Multimode Hexadecimal Addition and Subtraction in HN-OSSW

In this section, we use the proposed HN-OSSW to numerically demonstrate an ultrafast all-optical multimode hexadecimal addition and subtraction applying 16PSK signals, where the sixteen different phase symbols (0, $\pi/8$, $\pi/4$, $3\pi/8$, $\pi/2$, $5\pi/8$, $3\pi/4$, $7\pi/8$, π, $9\pi/8$, $5\pi/4$, $11\pi/8$, $3\pi/2$, $13\pi/8$, $7\pi/4$, $15\pi/8$) respectively correspond to the hexadecimal numbers (0, 1, 2, 3, 4, 5, 6, 7, 8, 9, a, b, c, d, e, f). As shown in Fig. 6, three 16PSK signals (A, B, C) are coupled into the HN-OSSW and carried on the excited TE_0 mode, meanwhile, two 16PSK signals (A, B) and a continuous wave (CW) are coupled into the HN-OSSW and carried on the excited TE_1 mode. With the high-performance three-input multimode FWM and taking into account the phase wrap of 2π, we simultaneously achieve six different hexadecimal addition and subtraction operations at various idlers on both modes, including A+B–C, C+A–B, C+B–A on TE_0 mode and A+B, A–B, B–A on TE_1 mode. Filtering and numerical analysis are followed by the mode demultiplexing to evaluate the performance of the logic operations.

The signal propagation and interaction in the HN-OSSW can be described by a multimode nonlinear Schrödinger equation (MM-NLSE) as follows [24], [36]:

$$\begin{aligned}\frac{\partial A_p(z,t)}{\partial z} &= D^{(p)}(z,t) + N^{(p)}(z,t) \\ &= i\left(\beta_0{}^{(p)} - \beta_0{}^*\right)A_p(z,t) - \left(\beta_1{}^{(p)} - \beta_1{}^*\right)\frac{\partial A_p(z,t)}{\partial t} + i\sum_{n^3 2}\frac{\beta_n{}^{(p)}}{n!}\left(i\frac{\partial}{\partial t}\right)^n A_p(z,t) \\ &\quad + i\frac{n_2\omega_0}{c}\sum_{l,m,n}\left\{\begin{array}{l} Q^{(1)}_{plmn}(\omega_0)\,2A_l(z,t)\,A_m(z,t)\,A_n^*(z,t) \\ +Q^{(2)}_{plmn}(\omega_0)\,2A_l^*(z,t)\,A_m(z,t)\,A_n(z,t)\end{array}\right\} \end{aligned} \quad (3)$$

Here, the propagation process is composed of two parts including $D^{(p)}(z,t)$ and $N^{(p)}(z, t)$, which respectively refer to the dispersive and the nonlinear parts of the MM-GNLSE for mode *p*. $D^{(p)}(z,t)$ could be expanded to the items expressed at the second line of Eq. 3, where A_P denotes the electric field envelope, $\beta_0{}^*$ and $\beta_1{}^*$ perform as the referenced propagation constant and first order dispersion at 1550 nm in the TE_0 mode. Thus, $\beta_0{}^{(p)}$–$\beta_0{}^*$ and $\beta_1{}^{(p)}$–$\beta_1{}^*$ are regarded as the relative propagation constant and first order dispersion. When n ≥ 2, $\beta_n{}^{(p)}$ becomes the nth-order dispersion of the HN-OSSW. In the simulation, β_2 and β_3 are all taken into account for each mode. The nonlinear part $N^{(p)}(z, t)$ couples the mode *p* to every combination of modes *l*, *m* and *n*. Particularly, $plmn = 1111$ represents the TE_0 mode while $plmn = 2222$ refers to the TE_1 mode. $Q^{(1)}{}_{plmn}$ and $Q^{(2)}{}_{plmn}$ denote the overlap integrals which greatly depend on the vectorial mode profiles of the HN-OSSW. As the polymer-filled gaps have a dominant impact on the nonlinear response, the nonlinear index n_2 in the equation is assumed to be the n_2 of MEH-PPV with the value of 2×10^{-16} m^2/W. The propagation losses of TE_0 and TE_1 modes are estimated as 4 dB/cm and 8 dB/cm [24], [36], respectively.

In the TE_0 mode, three 16-PSK signals (A, B and C) are generated by the pseudorandom binary sequences (PRBS) with the modulation rate of 160 Gbaud (640 Gb/s) at 1535.6 nm, 1542.8nm and 1571.6nm, respectively. The corresponding input average powers are properly amplified to 13dBm, 13dBm and 18dBm with ASE noise based on numerical EDFA model. For TE_1 mode, we replace signal C by a CW light and reduce the average power to 13 dBm. All the wavelengths of the inputs are maintained as those in the TE_0 mode. Considering both modes, the total operational speed then reaches up to 1.28 Tb/s. The influence of the nonlinear interaction length (L_{NL}) is analyzed in Fig. 7. Generally, one can find the FWM conversion efficiencies reach to the optimum as the L_{NL} is around 4 mm. For a shorter HN-OSSW, the accumulated nonlinear response is not enough to support a high-performance FWM, while for a longer one, the overall waveguide loss grows faster than the rising conversion efficiency, leading to a decline as the HN-OSSW continues increasing. The ripples found in Fig. 7(a) is attributed to the interference between the idler A+B-C and the cascading FWM idler generated by A and C+A-B. It is noted that the ripples in Fig. 7(a) are much more obvious than those in Fig. 7(b) and 7(c) because the idler A+B-C is much weaker (i.e., about -15dB) than A+C-B and B+C-A. This makes A+B-C be more sensitive to the other idlers generated by the cascade FWM. We then estimate the conversion efficiencies utilizing a strip silicon waveguide as a comparison. It is seen that with the HN-OSSW, we achieve at least 15 dB improvement for both modes.

The spectra of the multimode FWM with a 4-mm long HN-OSSW are illustrated in Fig. 8. Fig. 8(a) and 8(b) show the intramode FWM spectra which complete the hexadecimal addition/subtraction on different idlers at 1507.8 nm (A+B-C, A+B), 1564.4 nm (C+A-B, A-B) and 1578.8 nm (C+B-A, B-A). One can see that, in both figures, FWM efficiently occurs within each mode that strong idlers are successfully obtained. In specific, the corresponding average powers of the target idlers from short to long wavelength are calculated as -3.5 dBm, 12.2 dBm and 12.4 dBm, indicating the conversion efficiency higher than -22 dB. We then investigate the intermode FWM between TE_0 and TE_1 modes to estimate the crosstalk. In this case, signal A is carried on one mode, while B and C/CW are on the other. As shown in Fig. 8(c) and 8(d), idlers generated by the intermode FWM

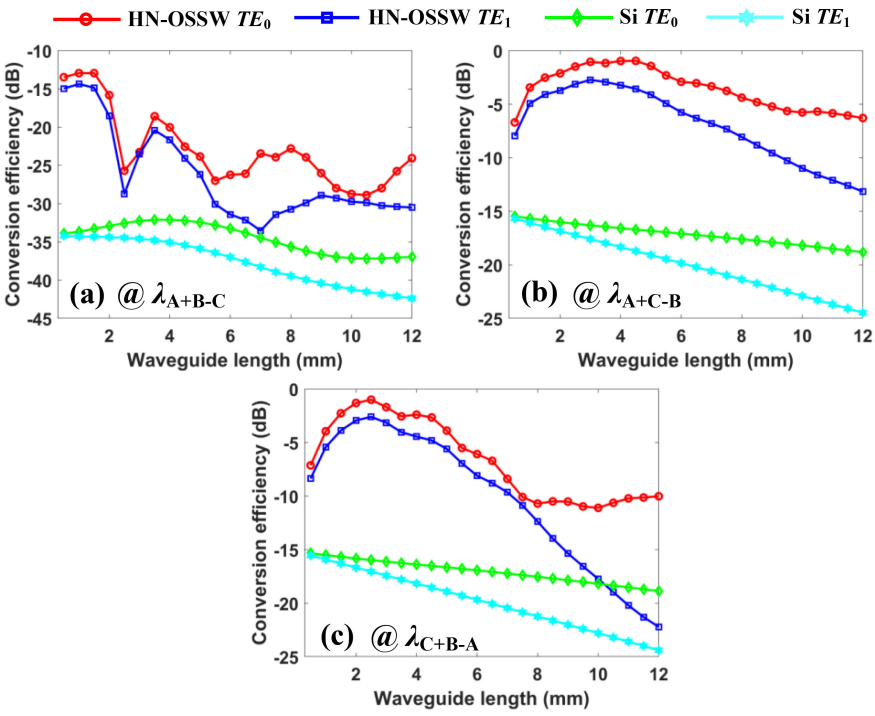

Fig. 7. Impact of the HN-OSSW length on the FWM conversion efficiency at different idlers.

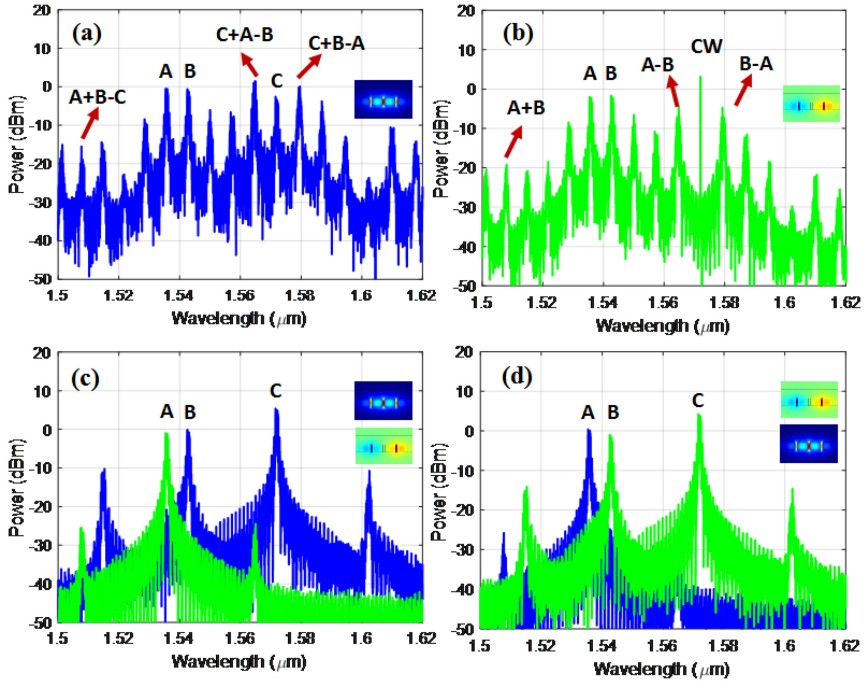

Fig. 8. Simulated spectra for the 1.28 Tb/s multimode hexadecimal addition and subtraction. (a) Intramode FWM for TE_0 mode. (b) Intramode FWM for TE_1 mode. (c) Intermode FWM for B, C/CW on TE_0 and A on TE_1 mode. (d) Intermode FWM for B, C/CW on TE_1 and A on TE_0 mode.

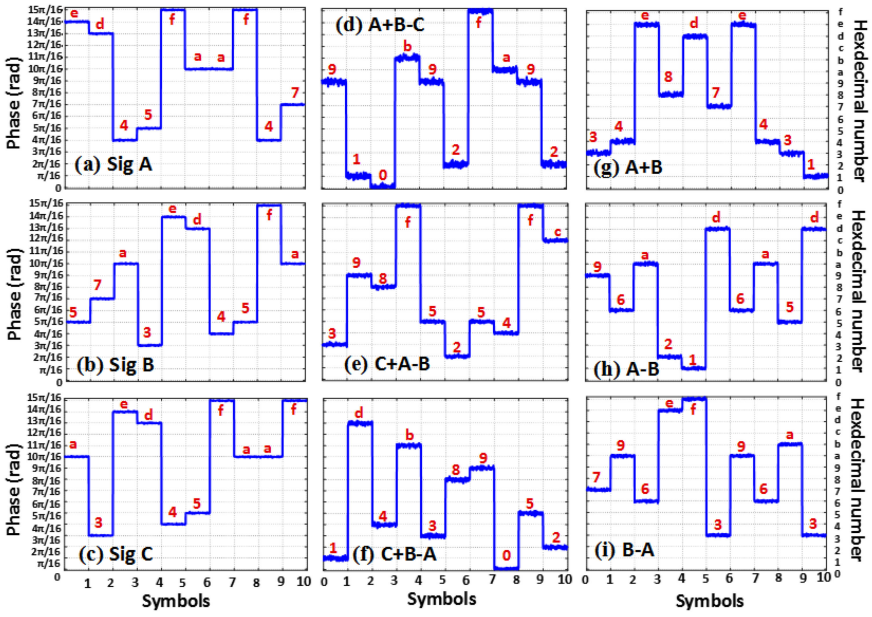

Fig. 9. Phase symbol sequences of the multimode hexadecimal addition and subtraction.

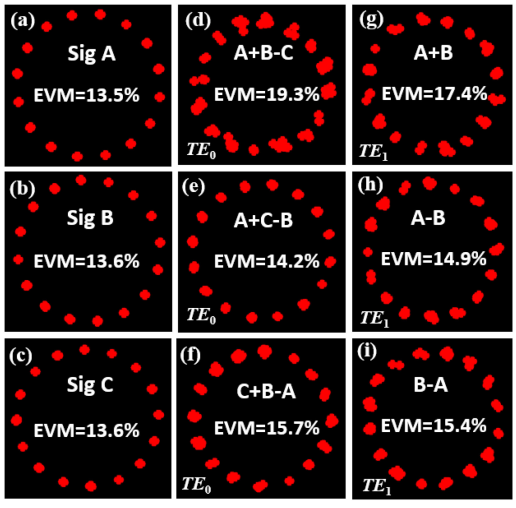

Fig. 10. Simulated constellations of the multimode hexadecimal addition and subtraction.

present an obvious deterioration about −10 dB compared to those of the intramode FWM, which suggests a slight crosstalk between different modes that can be totally ignorable in the simulation.

The idlers are then extracted by a tunable bandpass filter with the bandwidth of 6.4 nm and evaluated with an average power of 6 dBm. Fig. 9 shows the extracted symbol phase sequences of the multimode hexadecimal addition and subtraction. As shown in the figure, the phase statuses are clear and the logic operation results are correct, which well confirms the successful implementation of the mutimode hexadecimal addition and subtraction.

Additionally, to further evaluate the performance of the logic results, we investigate the constellations and calculate the corresponding optical signal-to-noise ratios (OSNRs) as well as the error vector magnitudes (EVMs) [38] of all idlers. As depicted in Fig. 10, the input signals exhibit a good quality with the OSNR over 30.3 dB, indicating the EVM around 13.5%. For the logic

results as shown in Fig. 10(d)-11(i), the logic results well maintain the signal formats composed of sixteen clear phase symbols. Meanwhile, A+C-B, C+B-A, A-B and B-A display better performances compared to those of A+B-C and A+B because the former corresponding idlers are much closer to the input signals, which is always accompanied with a higher FWM conversion efficiency. The respective OSNRs of A+B–C, C+A–B, C+B–A, A+B, A–B and B–A are estimated as 15.9 dB, 25.2 dB, 22.3 dB, 19.6 dB, 26.7 dB and 24.9 dB, resulting in the assessed EVMs of 19.3%, 14.2%, 15.7%, 17.4%, 14.9% and 15.4%. Thus, the highest EVM penalty here is estimated less than 5.8. Even though one can see some performance degradation associated with the accumulated noise and cascading FWM induced interference, the OSNR and EVM results still indicate that the proposed HN-OSSW is a potentially suitable candidate to enable ultrafast multimode optical computing. It is noted that, performance of the results can be further improved by employing the polymer with a higher nonlinear index or continuously narrowing the gap regions.

It is worth noting that the proposed HN-OSSW can totally replace the nonlinear element for generating canonical logic units (CLUs) to create a programmable logic array (CLUs-PLA) [26], [27]. Taking the mode number into account, the computing capacity, which is defined as the total amount of logic functions achieved by the optical PLA [26] would be further improved. Specifically, the computing capacity would be N times higher compared to that of the expanded CLUs-PLA reported in our previous work [26], where N is the mode number. In this scenario, high-performance multi-functional optical digital computing could be anticipated in a more compact way based on our proposed nanophotonic concept.

4. Conclusion

In summary, we have proposed a highly nonlinear organic silicon slot waveguide for FWM-based ultrafast multimode logic operations. Both TE_0 and TE_1 modes are well excited in the HN-OSSW. With the help of the highly nonlinear polymer MEH-PPV and the narrow gap regions, which intensively enhance the light confinement, the nonlinear coefficients of TE_0 and TE_1 modes are efficiently increased to 7078 $W^{-1}m^{-1}$ and 5858 $W^{-1}m^{-1}$, respectively. In addition, the influence of geometry on the nonlinear coefficients is discussed in detail. To further improve the multimode FWM efficiency, we investigate the phase mismatch evolutions depending on various gap and silicon rib widths. This optimization in turn promises an efficient intramode FWM but an ignorable intermode FWM crosstalk. Impacts of the coupling efficiency and nonlinear interaction length are also analyzed in detail. The possibility of the proposed HN-OSSW utilized in multimode ultrafast optical signal processing is then numerically demonstrated by a 1.28 Tb/s hexadecimal addition and subtraction. With the multimode non-degenerate FWM in the HN-OSSW between three-input 16-PSK signals, we simultaneously achieve six different hexadecimal logic operations including A+B-C, A+C-B, B+C-A, A+B, A-B and B-A. The achieved constellations are clear and the EVM penalties are less than 5.8 at the input OSNR of 30.3 dB. It is clearly seen that the proposed HN-OSSW has great potential for high-speed multimode logic operations and high-performance computing. More working modes can be anticipated based on the proposed structure or by further scaling the structure with more strip waveguides. This in turn requires additional well-designed directional couplers for mode multiplexing and demultiplexing. The increasing modes would enable a greater computing capacity. Moreover, with further optimization such as using other highly nonlinear polymer or narrowing the slot width, we can expect a device with a higher nonlinear coefficient, which provides a promising way for on-chip high-capacity all-optical signal processing.

References

[1] D. J. Richardson, J. M. Fini, and L. E. Nelson, “Space-division multiplexing in optical fibres,” *Nat. Photon.*, vol. 7, no. 5, pp. 354–362, 2013.
[2] H. R. Stuart, “Dispersive multiplexing in multimode optical fiber,” *Science*, vol. 289, no. 5477, pp. 281–283, 2000.
[3] I. N. Papadopoulos, S. Farahi, C. Moser, and D. Psaltis, “Focusing and scanning light through a multimode optical fiber using digital phase conjugation,” *Opt. Exp.*, vol. 20, no. 10, pp. 10583–10590, 2012.

[4] A. Mecozzi, C. Antonelli, and M. Shtaif, "Nonlinear propagation in multi-mode fibers in the strong coupling regime," *Opt. Exp.*, vol. 20, no. 11, pp. 11673–11678, 2012.
[5] A. D. Ellis, N. M. Suibhne, F. G. Gunning, and S. Sygletos, "Expressions for the nonlinear transmission performance of multi-mode optical fiber," *Opt. Exp.*, vol. 21, no. 19, pp. 22834–22846, 2013.
[6] C. Li, D. Liu, and D. Dai, "Multimode silicon photonics," *Nanophotonics*, vol. 8, no. 2, pp. 227–247, 2018.
[7] D. Dai, J. Wang, and S. He, "Silicon multimode photonic integrated devices for on-chip mode-division-multiplexed optical interconnects," *Prog. Electromagn. Res.*, vol. 143, pp. 773–819, 2013.
[8] B. Stern *et al.*, "On-chip mode-division multiplexing switch," *Optica*, vol. 2, no. 6, pp. 530–535, 2015.
[9] J. Leuthold, C. Koos, and W. Freude, "Nonlinear silicon photonics," *Nat. Photon.*, vol. 4, no. 8, pp. 535–544, 2010.
[10] Q. Lin, O. J. Painter, and G. P. Agrawal, "Nonlinear optical phenomena in silicon waveguides: Modeling and applications," *Opt. Exp.*, vol. 15, no. 25, pp. 16604–16644, 2007.
[11] C. Koos, L. Jacome, C. Poulton, J. Leuthold, and W. Freude, "Nonlinear silicon-on-insulator waveguides for all-optical signal processing," *Opt. Exp.*, vol. 15, no. 10, pp. 5976–5990, 2007.
[12] E. Timurdogan, C. V. Poulton, M. J. Byrd, and M. R. Watts, "Electric field-induced second-order nonlinear optical effects in silicon waveguides," *Nat. Photon.*, vol. 11, no. 3, pp. 200–206, 2017.
[13] Y. Mao, B. Liu, R. Ullah, T. Sun, and L. Zhao, "All-optical XOR function accompanied with OOK/PSK format conversion with multicast functionality based on cascaded SOA configuration," *Opt. Commun.*, vol. 466, Art. no. 125421, 2020.
[14] I. Rendón-Salgado, E. Ramírez-Cruz, and R. Gutiérrez-Castrejón, "640 Gb/s all-optical and gate and wavelength converter using bulk SOA turbo–switched Mach–Zehnder interferometer with improved differential scheme," *Opt. Laser Technol.*, vol. 109, pp. 671–681, 2019.
[15] K. Li, H. F. Ting, M. A. Foster, and A. C. Foster, "High-speed all-optical NAND/AND logic gates using four-wave mixing Bragg scattering," *Opt. Lett.*, vol. 41, no. 14, pp. 3320–3323, 2016.
[16] K. Maji, K. Mukherjee, and A. Raja, "Frequency encoded all-optical universal logic gates using terahertz optical asymmetric demultiplexer," *IJPOT*, vol. 4, no. 3, pp. 1–7, 2018.
[17] P. Rani, Y. Kalra, and R. K. Sinha, "Design of all optical logic gates in photonic crystal waveguides," *Optik*, vol. 126, no. 9, pp. 950–955, 2015.
[18] A. G. Coelho Jr, M. B. C. Costa, A. C. Ferreira, M. G. Da Silva, M. L. Lyra, and A. S. B. Sombra, "Realization of all-optical logic gates in a triangular triple-core photonic crystal fiber," *J. Lightw. Technol.*, vol. 31, no. 5, pp. 731–739, 2013.
[19] Y. Mao *et al.*, "All-optical 3R regeneration for DPSK signal based on a semiconductor optical amplifier scheme," *Appl. Opt.*, vol. 59, no. 12, pp. 3526–3529, 2020.
[20] L. Lei, J. Dong, B. Zou, Z. Wu, W. Dong, and X. Zhang, "Expanded all-optical programmable logic array based on multi-input/output canonical logic units," *Opt. Exp.*, vol. 22, no. 8, pp. 9959–9970, 2014.
[21] L. Lei, J. Dong, Y. Yu, S. Tan, and X. Zhang, "All-optical canonical logic units-based programmable logic array (CLUs-PLA) using semiconductor optical amplifiers," *J. Lightw. Technol.*, vol. 30, no. 22, pp. 3532–3539, 2012.
[22] J. Mata *et al.*, "Artificial intelligence (AI) methods in optical networks: A comprehensive survey," *Opt. Switching Netw.*, vol. 28, pp. 43–57, 2018.
[23] J. Wang *et al.*, "Dual-Channel and logic gate based on four-wave mixing in a multimode silicon waveguide," *IEEE Photon. J.*, vol. 9, no. 4, Aug. 2017, Art. no. 7802806.
[24] Y. Ding, J. Xu, H. Ou, and C. Peucheret, "Mode-selective wavelength conversion based on four-wave mixing in a multimode silicon waveguide," *Opt. Exp.*, vol. 22, no. 1, pp. 127–135, 2014.
[25] Y. Qiu *et al.*, "Mode-selective wavelength conversion of OFDM-QPSK signals in a multimode silicon waveguide," *Opt. Exp.*, vol. 25, no. 4, pp. 4493–4499, 2017.
[26] L. Lei, J. Dong, B. Zou, Z. Wu, W. Dong, and X. Zhang, "Expanded all-optical programmable logic array based on multi-input/output canonical logic units," *Opt. Exp.*, vol. 22, no. 8, pp. 9959–9970, 2014.
[27] W. Dong, J. Hou, and X. Zhang, "Investigation on expanding the computing capacity of optical programmable logic array based on canonical logic units," *J. Lightw. Technol.*, vol. 36, no. 18, pp. 3949–3958, 2018.
[28] S. J. Martin, D. D. C. Bradley, P. A. Lane, H. Mellor, and P. L. Burn, "Linear and nonlinear optical properties of the conjugated polymers PPV and MEH-PPV," *Phys. Rev. B*, vol. 59, no. 23, 1999, Art. no. 15133.
[29] K. Debnath, A. Z. Khokhar, G. T. Reed, and S. Saito, "Fabrication of arbitrarily narrow vertical dielectric slots in silicon waveguides," *IEEE Photon. Technol Lett.*, vol. 29, no. 15, pp. 1269–1272, 2017.
[30] P. A. Anderson, B. S. Schmidt, and M. Lipson, "High confinement in silicon slot waveguides with sharp bends," *Opt. Exp.*, vol. 14, no. 20, pp. 9197–9202, 2006.
[31] C. Koos *et al.*, "All-optical high-speed signal processing with silicon–organic hybrid slot waveguides," *Nat. Photon.*, vol. 3, no. 4, pp. 216–219, 2009.
[32] M. P. Nielsen, X. Shi, P. Dichtl, S. A. Maier, and R. F. Oulton, "Giant nonlinear response at a plasmonic nanofocus drives efficient four-wave mixing," *Science*, vol. 358, no. 6367, pp. 1179–1181, 2017.
[33] R. F. Oulton, G. Bartal, D. F. P. Pile, and X. Zhang, "Confinement and propagation characteristics of subwavelength plasmonic modes," *New J. Phys.*, vol. 10, no. 10, 2008, Art. no. 105018.
[34] M. Samoc, A. Samoc, and B. Luther-Davies, "Third harmonic autocorrelation and wave mixing in a thin film of poly(p-phenylenevinylene)," *Opt. Exp.*, vol. 11, no. 15, pp. 1787–1792, 2003.
[35] H. Haus, W. Huang, S. Kawakami, and N. Whitaker, "Coupled-mode theory of optical waveguides," *J. Lightw. Technol.*, vol. 5, no. 1, pp. 16–23, 1987.
[36] F. Poletti and P. Horak, "Description of ultrashort pulse propagation in multimode optical fibers," *J. Opt. Soc. Am. B*, vol. 25, no. 10, pp. 1645–1654, 2008.
[37] K. Debnath, A. Z. Khokhar, S. A. Boden, S. Z. Oo, H. M.Chong, and S. Saito, "Low-loss slot waveguides with silicon (111) surfaces realized using anisotropic wet etching," *Frontiers in Materials*, vol. 3, no. 51, 2016.
[38] R. Schmogrow *et al.*, "Error vector magnitude as a performance measure for advanced modulation formats," *IEEE Photon. Technol. Lett.*, vol. 24, no. 1, pp. 61–63, Jan. 2012.